Facile Synthesis of Fe-Loaded Mesoporous Silica by a Combined Detemplation−Incorporation Process through Fenton's Chemistry

Yong-Mei Liu, Jie Xu, Lin He, Yong Cao,* He-Yong He, Dong-Yuan Zhao, Ji-Hua Zhuang,* and Kang-Nian Fan

Department of Chemistry and Shanghai Key Laboratory of Molecular Catalysis and Innovative Materials, Fudan University, Shanghai 200433, People's Republic of China

Received: March 13, 2008; Revised Manuscript Received: August 4, 2008

The present work describes a new approach to synthesize Fe species within the channels of mesoporous SBA-15 silica using Fenton's reagent (Fe^{2+}-H_2O_2) as an iron precursor. For the first time Fe ions were incorporated within as-synthesized surfactant-containing mesoporous host by a simultaneous detemplation and Fe-incorporation process at low temperature. The resulting materials were characterized by X-ray diffraction (XRD), thermogravimetric differential thermal analysis, N_2 sorption, DRIFTS, transmission electron microscopy (TEM), UV−vis diffuse reflectance spectroscopy, UV Raman, X-ray photoelectron spectroscopy, and Friedel−Crafts alkylation catalysis. The ordered mesostructure of the SBA-15 host is retained as indicated by XRD and HRTEM, and the surface areas of the Fe-SBA-15 materials are in the range of 640−853 $m^2\ g^{-1}$ comparable to 784 $m^2\ g^{-1}$ for the calcined host. The characterization results also indicate the presence of iron species inside the silica pores, as well as a good dispersion of the iron oxide nanoclusters within the pores of the host material. Controlled iron loading was possible to a maximum of 9 wt %. The catalyst shows significantly enhanced performance on benzylation of benzene using benzyl chloride as the alkylating agent compared to conventionally prepared Fe/SBA-15.

1. Introduction

Ordered mesoporous silica (OMS) have attracted tremendous interest in the past decade owing to their broad applications in heterogeneous catalysis, host−guest chemistry, chemical sensors, adsorption, separation, environmental technology, and as electrodes in solid-state ionic devices.[1,2] In 1992, Mobil researchers first reported the synthesis of the M41S family of mesoporous silica materials via a surfactant-templated sol−gel process.[3,4] Since then, much attention has been directed toward the synthesis of numerous different mesoporous materials with different pore structures and compositions by changing the surfactants or inorganic precursors.[5−7] Recently, SBA-15, another new type of ordered mesoporous material, achieved by using amphiphilic triblock copolymers as a structure-directing agent in highly acidic media, has attracted considerably more attention.[8,9] SBA-15 material possesses a high surface area and uniform tubular channels with tunable pore diameters in the range of 5−30 nm, which are significantly larger than those of MCM-41 materials. Especially due to its thicker walls, SBA-15 provides a thermal stability and hydrothermal stability that far exceed those for MCM-41 with thinner walls.[8,10] All these properties of SBA-15 material make it appealing as a more suitable candidate for catalytic applications.[8−12]

The most significant disadvantage of the SBA-15 material, however, is that there are few catalytically active sites on its amorphous SiO_2 wall.[13] This is in contrast to the fact that zeolites usually possess a large number of isolated active sites.[14,15] The introduction of metal ion other than Si^{4+} is thus required to use SBA-15 as a possible catalyst.[16] Many different synthetic procedures have been developed to incorporate transition metals such as aluminum, titanium, vanadium, gallium, tin, tungsten, manganese, and iron into mesoporous SBA-15 materials.[16−21] One of the most popular methods of incorporating metals into mesoporous silica is the direct hydrothermal (DHT) method, which consists of the direct addition of metal ion precursors to the synthesis gel before the hydrothermal reaction takes place.[18,22] Other methods, such as conventional wet impregnation and grafting,[12,23,24] have also been used. However, these methods have presented general problems, which include the loss of the ordered mesoporous structure, low metal loadings, or formation of bulk species outside the silica host.[25]

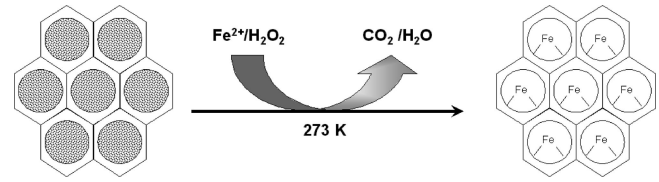

Figure 1. Schematic illustration for preparing Fe-loaded SBA-15 via the detemplation−incorporation process through Fenton's chemistry.

In the present work, we report for the first time Fe ions being incorporated into surfactant-containing mesoporous silica pores. Fenton's reagent (Fe^{2+}−H_2O_2) processing, previously established to be an effective method for treating industrial organic pollutants,[26−28] has shown to be particularly useful in synthesizing Fe species within the channels of mesoporous SBA-15 silica. Our results have shown that, by treating as-synthesized parent SBA-15 with a Fenton's reagent (Fe^{2+}−H_2O_2)[26] at low temperature, a facile simultaneous detemplation and Fe incorporation into the mesoporous silica materials can be achieved (Figure 1). The introducing of Fe ions into SBA-15 materials opens new opportunities for further synthesis of ferric oxide materials in confined environments and their use in catalytic applications. The method described in this work is a simple and new approach for the synthesis of Fe species in mesoporous silica materials.

* To whom correspondence should be addressed. E-mail: yongcao@fudan.edu.cn (Y.C.); jihuaz@fudan.edu.cn (J.-H.Z.).

10.1021/jp802202v CCC: $40.75
Published on Web 09/25/2008

2. Experimental Section

2.1. Synthesis of SBA-15. Pure siliceous SBA-15 samples were synthesized using the technique reported by Zhao et al.[8] Triblock copolymer Pluronic P123 (EO_{20}-PO_{70}-EO_{20}, Aldrich) was used as a polymeric template. In a typical synthesis, 2.0 g of Pluronic P123 was dissolved in the mixture of 15 mL of water and 60 mL of 2 M HCl with stirring, and then 4.25 g of tetraethyl orthosilicate (TEOS, Aldrich) was added. The resulting reaction mixture was stirred at 313 K for 5 h and then hydrothermally treated at 368 K for 72 h under static conditions in a Teflon-lined stainless steel autoclave. The solid product was filtered, washed with distilled water, and dried in air at 353 K overnight.

2.2. Synthesis of Fe-SBA-15. A series of Fe-SBA-15 samples were prepared as follows: As-synthesized P123 containing SBA-15 (2.0 g) was stirred with 200 mL of distilled water containing 50 mL of Fe^{2+} solution (0.1−0.5 M) in a three-necked flask equipped with a condenser. To this suspension, 50 mL 30% H_2O_2 was added dropwise. The solution was stabilized by cooling down in ice water since the propagation of the $OH^{\bullet}$ radicals was very fast, which could increase the temperature tremendously.[26] The removal of the template was visually observed by the evolution of a dense fog through the coil condenser. The reaction was ended after stirring for 2 h. The suspension was filtered off and the solid dried at 393 K overnight. The resultant samples were referred to as Fe-SBA(n) (n = 1, 2, 4, 9), where n was the Fe content in the Fe-loaded catalysts. For comparison, a reference Fe-loaded catalyst denoted as Fe/SBA(n) was prepared by incipient wetness of a conventional 873 K calcined SBA-15 with iron(III) nitrate solutions.

2.3. Characterization. Powder X-ray diffraction (XRD) analysis was performed using a Germany Bruker D8Advance X-ray diffractometer with Cu Kα radiation (40 kV, 40 mA), 0.02° step size, and 1-s step time. Nitrogen sorption isotherms and textural properties of the materials were determined at 77 K using nitrogen in a conventional volumetric technique by a Micromeritics TriStar 3000 equipment. Before the analysis, the samples were evacuated for 12 h at 423 K under vacuum. The surface area was calculated using the Brunauer−Emmett−Teller (BET) method based on adsorption data in the partial pressure (P/P_0) range 0.05−0.2, and total pore volume was determined from the amount of the nitrogen adsorbed at P/P_0 of ca. 0.99. The elemental composition was determined by inductively coupled plasma atomic emission spectroscopy (ICP-AES) after the sample was dissolved in a mixture of HF and HNO_3. Thermogravimetric analysis (TGA) was performed using a Perkin-Elmer TGA 7 analyzer with a heating rate of 20 K·min^{-1} under an air flow of 30 mL·min^{-1}. Diffuse reflectance infrared Fourier transform spectra (DRIFTS) were recorded using a Bruker Vector 22 spectrometer equipped with a deuterated triglycine sulfate (DTGS) detector and a KBr beam splitter. The samples were placed in a sample cup inside a Harrick diffuse reflectance cell equipped with ZnSe windows and a thermocouple mount that allowed direct measurement of the sample temperature. All spectra were collected in dry air atmosphere at 373 K.

Transmission electron microscopy (TEM) images were recorded digitally on a JEOL 2011 electron microscope operating at 200 kV. Energy dispersion spectrum (EDS) was obtained from an attached Oxford Link ISIS energy-dispersive spectrometer fixed on the JEM-2011 electron microscope. Diffuse reflectance UV−vis spectra were collected on a Varian Cary 5 spectrophotometer equipped with a "Praying Mantis" attachment from Harrick. The sample cell was equipped with a heater unit, a thermocouple, and a gas flow system for *in situ* measurements. The samples were dehydrated in dry air at 673 K for 30 min on line. The spectra were recorded upon cooling down to room temperature, flowing dry air through the sample to avoid the rehydration processes. UV-Raman measurements were carried out using the UV line at 325 nm from a Kimmon IK3201R-F He−Cd laser as the exciting source, where a laser output of 30 mW was used and the maximum incident power at the sample was approximately 6 mW. X-ray photoelectron spectroscopy (XPS) data were collected on a Perkin-Elmer PHI 5000C spectrometer equipped with a SPECS EA10 MCD hemispherical analyzer. The samples were pressed in indium foil to minimize charging. Narrow and wide scans of all elements were collected for the prominent photoelectron transitions and X-ray-excited Auger transitions.

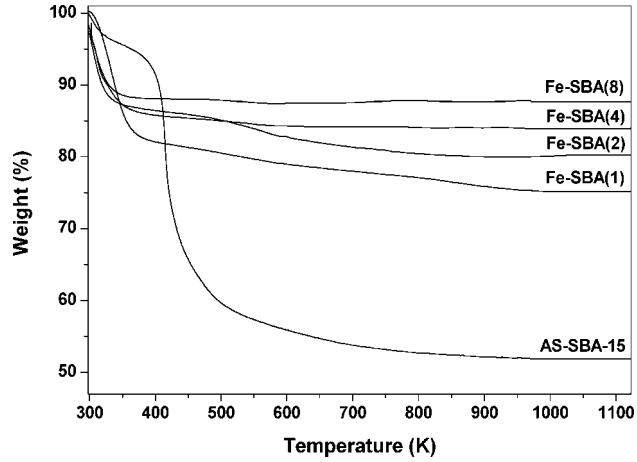

Figure 2. TGA curves of as-synthesized SBA-15 and detemplated Fe-loaded SBA-15 samples via Fenton oxidation.

2.4. Catalytic Studies. Anhydrous AR grade chemicals were used without further purification. The liquid-phase benzylation of benzene with benzyl chloride (BC) was carried out in a 50-mL three-necked flask equipped with a condenser and a septum. The temperature of the reaction vessel was maintained using an oil bath. In a typical run, benzene and BC were added (the molar ratio of benzene to BC was 15) to the activated catalyst. The catalysts were activated at 473 K in air for 4 h with a flow rate of 50 mL· min^{-1} and cooled to room temperature prior to their use in the reaction. The reaction mixture was magnetically stirred (800 rpm) and heated to the required temperature under atmospheric pressure. Samples were withdrawn at regular intervals and analyzed using a gas chromatograph (Trace GC Ultra) equipped with a FID detector and a capillary column. The products were also identified by gas chromatography mass spectrometry (GC-MS) analysis. Since benzene was used in excess, conversion was calculated based on the benzylating reagent, i.e., BC.

3. Results and Discussion

3.1. Structural Characteristics of Fe-SBA-15. The effectiveness of the detemplation can be demonstrated by TGA (Figure 2). Two major weight loss processes can be observed for all five samples. The weight loss below 423 K can be attributed to the desorption of physisorbed water.[29] The weight loss between 423 and 1123 K corresponds to the decomposition of organic templates and the release of water formed during the condensation of silanols in the silica framework.[30] The weight loss for as-synthesized SBA-15 at temperatures between 423 and 1123 K is ca. 41.6 wt %, which is similar to the content

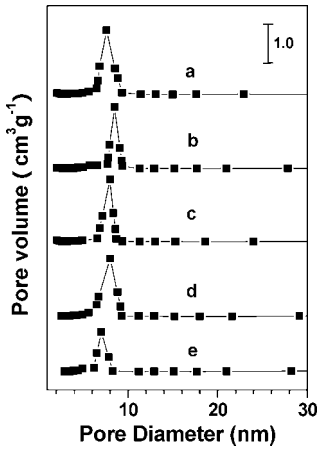

Figure 3. Pore size distribution (PSD) for (a) cal-SBA-15, (b) Fe-SBA(1), (c) Fe-SBA(2), (d) Fe-SBA(4), (e) Fe-SBA(8).

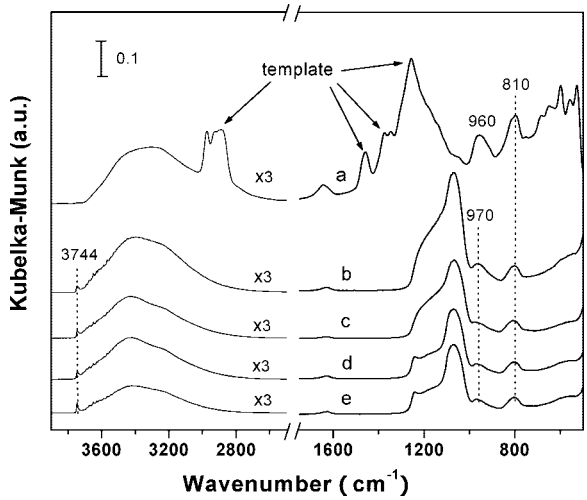

Figure 4. DRIFT spectra of various Fe-loaded SBA-15 materials: (a) AS-SBA-15, (b) Fe-SBA(1), (c) Fe-SBA(2), (d) Fe-SBA(4), (e) Fe-SBA(8).

of the ionic surfactant template in typical MCM-41 and MCM-48 silicas.[8,31] It is evident that, after the treatment with $Fe^{2+}-H_2O_2$ combination, the organic templates are removed completely from SBA-15. Moreover, it is found that the amount of physisorbed water in the treated samples (ca. 10−17 wt %) is significantly larger than for the calcined SBA-15 material (ca. 5 wt %). This is an indirect proof that mesoporosity has been developed and water enters into the channels.[32] Mesoporosity formation was confirmed by nitrogen adsorption−desorption measurements. The pore-size distribution, calculated according to the BJH method from the adsorption branch of the isotherms,[29,32] confirms the presence of mesoporosity in the $Fe^{2+}-H_2O_2$ treated material. A pronounced development of a pore-size distribution between 6 and 10 nm with a maximum at ca. 8 nm, characteristic of ordered hexagonal channels is observed (Figure 3).

The absence of triblock copolymer template in the $Fe^{2+}-H_2O_2$ treated samples can be further confirmed by the infrared spectroscopy (IR) analysis (Figure 4). The C−H stretching and C−H bending or deformation vibrations at around 2850−2900 and 1240−1500 cm^{-1} are clearly observed in the as-synthesized SBA-15 sample. However, these characteristic bands are totally absent in the Fe-SBA(n) samples. This suggests the efficient removal of the organic template by the Fenton processing.[32] In contrast to the as-synthesized SBA-15, the typical bands due

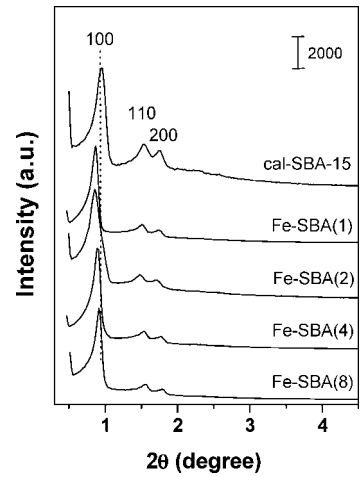

Figure 5. Low-angle X-ray diffraction patterns of various Fe-doped SBA-15 materials.

to siliceous material Si−O−Si, i.e., a main band at 1070 cm^{-1}, with a shoulder at 1200 cm^{-1}, due to asymmetric Si−O−Si stretching modes, as well as the corresponding symmetric stretch at 810 cm^{-1},[33,34] are observed for the Fe-SBA samples. More importantly, a significant modification in the Si−O−Si bending bands at around 960 cm^{-1}, indicative of Si−O−Fe species, is identified for the Fe-containing samples with Fe content up to 9.0 wt %. It is also worthwhile to note that the spectrum in the hydroxyl region of the Fe-SBA(n) samples display a narrow vibration band at 3740 cm^{-1} belonging to isolated terminal silanol groups and a broad absorption band between 3700 and 3300 cm^{-1} (centered at ca. 3660 cm^{-1}) due to OH-stretching vibrations of geminal and associated terminal silanol groups,[35,36] giving evidence the presence of a high abundance of silanol groups on the pore wall surface.

XRD patterns obtained for calcined SBA-15 and as-synthesized Fe-SBA(n) with different loading materials are depicted in Figure 5. All the materials show well-defined XRD patterns corresponding to typical SBA-15 structures, implying the overall mesoporous hexagonal structure after Fe incorporation is retained. A shift of the diffraction peaks to lower 2θ values is identified for the Fe-SBA samples, possibly due to a less structural shrinkage during the low-temperature template removal step.[12] Moreover, no additional diffraction peaks due to iron oxide phases are observed at high angles ($2\theta > 5°$). The relative intensities of the 100 diffraction for Fe-SBA-15, listed in Table 1, indicate that no significant destruction occurred during the Fenton treatment process. More interestingly, all the samples, except for the sample containing 8.9 wt % Fe, showed a slight increase in the intensity of the d_{100} peak. The hexagonal arrangement of the SBA-15 frameworks is retained even after iron incorporation with high Fe content, as could be seen from TEM and N_2-adsorption data presented as follows. It is suggested that the iron species are well-dispersed on the channels of SBA-15. Thus, the slight reduction of the 100 reflections in the higher loaded Fe-SBA(8) sample is more likely due to a dilution of silica with increased incorporation of iron oxide as a consequence of higher adsorption factor for X-rays than silicon.[12,37]

Figure 6 and Table 1 show the N_2 sorption results obtained for the calcined SBA-15 and as-synthesized Fe-SBA(n) samples. All isotherms are of type IV, according to the IUPAC classification, and exhibit an H1 type broad hysteresis loop, which is typical of large-pore mesoporous solids.[8] As the relative pressure increases ($P/P_0 > 0.6$), all isotherms exhibit a sharp

TABLE 1: Physicochemical Properties of SBA-15 and Fe-SBA Materials

sample	S_{BET}[a] ($m^2\ g^{-1}$)	V[a] ($cm^3\ g^{-1}$)	D_{BJH}[a] (nm)	a_0[a]	d_{100} intensity	ICP Fe (wt %)	XPS Fe %[b]	Fe 2p binding energy (eV)
AS-SBA-15	108							
Cal-SBA-15	784	1.07	7.6	10.6	100			
Fe-SBA(1)	853	1.23	8.5	11.8	104	1.2	1.0(102)	710.9
Fe-SBA(2)	826	1.21	8.3	11.8	104	1.9	2.0(51)	710.5
Fe-SBA(4)	805	1.21	8.0	11.5	103	4.1	4.3(18)	710.6
Fe-SBA(8)	760	1.20	7.0	11.1	97	8.9	7.4(12)	710.7
Fe/SBA(4)	528	0.89	6.1	10.3	96	4.2	3.5(25)	711.0(712.9)
Fe-SBA(4)-C	790	1.16	7.8	10.8	98	4.1	4.3(20)	710.5

[a] S_{BET}, BET surface area; V, total pore volume; D_{BJH}, pore diameter, calculated from the adsorption branch with the BJH method; a_0, cell constant $a_0 = 2d_{100}/\sqrt{3}$. [b] The data included in parenthesis is the Si/Fe atomic ratio calculated from XPS data.

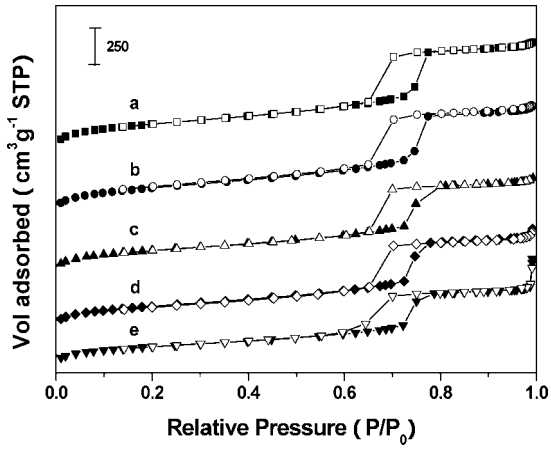

Figure 6. Nitrogen sorption isotherms for (a) cal-SBA-15, (b) Fe-SBA(1), (c) Fe-SBA(2), (d) Fe-SBA(4), (e) Fe-SBA(8).

step characteristic of capillary condensation of nitrogen within uniform mesopores. With increasing Fe content, the pore volume is almost remained about 1.2 $cm^3\ g^{-1}$, and the specific surface area is between 853 and 760 $m^2\ g^{-1}$ (Table 1). The pore volume and the specific surface area of sample Fe-SBA(4) is obviously larger than that of the impregnation-derived Fe/SBA(4) sample, suggesting that the new method shows many benefits such as larger surface areas and pore volume. More importantly, reducing the number of steps will contribute to an improved and faster synthesis process. By using this technology high-temperature calcinations are avoided, which leads to savings in operational costs (less energy input) and less investment for equipment.

TEM images and EDS spectrum for the Fe-SBA(8) sample as an example show the regular hexagonal array of uniform channels (Figure 7), revealing that the highly ordered pore structure of the host material has been preserved during the iron incorporation process. No bulk aggregation is observed inside and outside of the pores. However, a strong signal for iron in the EDS data demonstrates that Fe is present. Thus, together with the high-angle XRD evidence (see the Supporting Information), it can be concluded that iron oxides exist in the pores of host silica in nanometer small clusters. The Fe content as determined by elemental analysis using ICP (Table 1) was 1.2, 1.9, 4.1, and 8.9 wt % for Fe-SBA(l), Fe-SBA(2), Fe-SBA(4), and Fe-SBA(8), respectively. Note that a high Fe content almost up to 9 wt % could be well incorporated into the matrix of the SBA-15 material. This value is much higher than those reported for Fe-SBA-15 synthesized by direct hydrothermal and template ion-exchange methods.[18,22,38]

3.2. Chemical States of Fe Species. UV−vis spectroscopy has been used extensively to characterize the nature and coordination of Fe^{3+} ions in Fe-substituted molecular sieves.[39,40] Figure 8 shows UV−vis DRS spectra of as-synthesized Fe-SBA samples with different Fe loading. No significant absorption at or above 400 nm is observed for Fe-SBA samples with Fe loadings of up to 8.9 wt %, indicating that the as-synthesized materials are free from bulk ferric oxide.[40] The spectra show a characteristic absorption band around 245 nm; the intensity of this band increases with increasing iron content of the material. A deconvolution of this band reveals two main absorption features at 245 and 270 nm corresponding to tetrahedral framework Fe^{3+} species and isolated extraframework iron species in an octahedral or pseudotetrahedral environment in SBA-15, respectively.[41] As the iron content increases, an increase of the intensity of the band at 270 nm is observed with respect to the absorption appearing at 240 nm, resulting in a progressive shift of the overlapping band toward a higher wavelength. In addition, a new feature at 385 nm appears for the sample with 8.9 wt % Fe loading, suggesting the presence of small oligomeric Fe_xO_y clusters due to a further polymerization of the Fe species.[40,41] It is worth noting that the spectrum of impregnation-derived Fe/SBA(4) shows additional bands around 450 nm arising from "bulklike" Fe_2O_3 crystallites (inset to Figure 8). The absence of this species in Fe-SBA(4) material indicates a much higher metal oxide dispersion achieved by using the Fenton-incorporation method. So it can conclude that this method allows the controlled dispersion of a higher amount of iron oxide species on the surface of the mesoporous host, thus providing a new, attractive alternative for preparing defined transition metal modified mesoporous catalyst with more favorable.

UV resonance Raman spectroscopy has recently shown to be very powerful for the study of various catalytic materials, especially for the identification of the molecular structure of isolated transition metal atoms anchored on the surface of zeolites or related materials.[12,43] Figure 9 shows the UV Raman spectra of the Fe-containing samples excited by the 325-nm line. Four Raman bands at 490, 600, 800, and 978 cm^{-1} are observed on the spectrum of pure siliceous SBA-15 sample. The bands at 490 and 600 cm^{-1} are assigned to the three and four silane rings and the band at 800 cm^{-1} is ascribed to the vibration mode of siloxane linkage.[20,43] The band at 978 cm^{-1} is associated with the Si−O−Si bond near the framework iron species or other defect site such as the surface silanol groups.[20] Compared with the pure siliceous SBA-15, a new band at 1075 cm^{-1} is detected for Fe substituted SBA-15 materials. This band is assigned to the Fe−O−Si asymmetric stretching mode of the isolated tetrahedral iron ions in the silica framework, in agreement with previous studies on Fe-containing MCM-41 materials.[42] Notice that the characteristic Fe−O−Si Raman bands are not detected for the Fe/SBA(4) sample. By consideration of the results of diffuse reflectance UV−vis spectra, this fact may be due to the

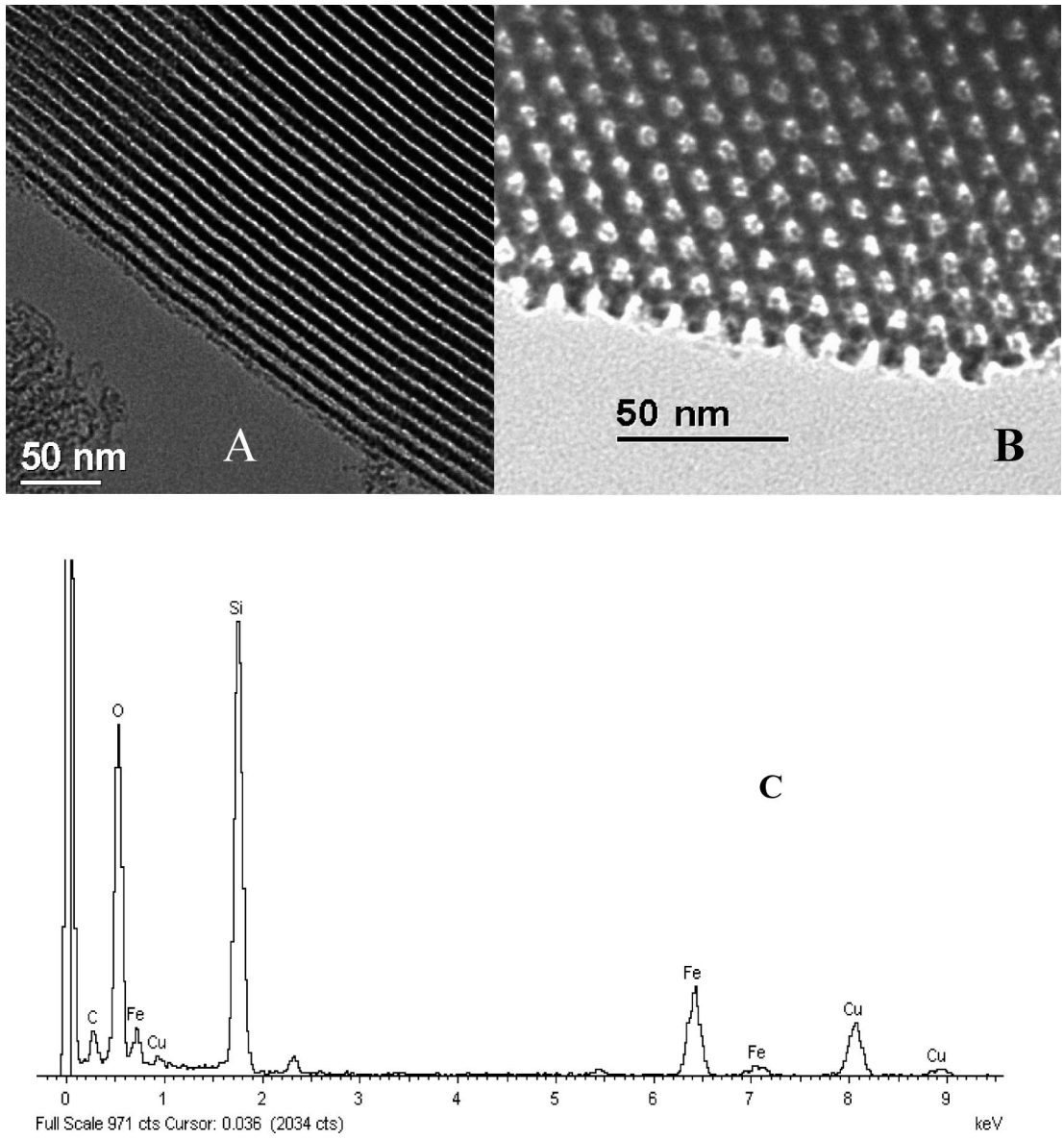

Figure 7. High-resolution TEM photos with the electron beam perpendicular (A) and parallel (B) to the pore channels and EDS spectrum (C) of sample Fe-SBA(8) collect from the former region.

existence of substantial amount of large size iron species or iron oxides in the channels.[41]

XPS was used to analyze the binding energy (BE) values and the nature and coordination of the corresponding elements present in Fe-SBA-15. Figure 10 compares the Fe 2p spectra of the Fe-SBA(4) and Fe/SBA(4) samples. As can be seen in Figure 10, both samples had two sharp peaks with binding energy values of 710.9 and 723.7 eV. In the case of Fe/SBA(4), a shoulder peak with the binding energy of 712.9 eV is observed. The Fe 2p peak at 710.0 eV is typically assigned for the iron atom with +3 coordination state. Similar results have also been reported in the iron-substituted mesoporous silica materials. Further, the shoulder peak in the Fe/SBA(4) at 712.9 eV can be assigned to small iron oxide particles, which normally have binding energy values of 710.7 and 712 eV.[43] This allows further confirmation that the Fe/SBA(4) sample contain considerable amount of octahedral coordinated iron atoms. In addition, the broad peak, which is centered at 723.7 eV, may be assigned to iron atoms coordinated to hydroxyl groups or water molecules in the samples. The XPS intensity ratio of Fe 2p/Si 2s values for various Fe-SBA-15 samples is also included in Table 1, which reflects the iron dispersion on mesoporous silica support. Except for that of the Fe/SBA(4) sample, the surface atomic ratio of Fe/Si is in close agreement with the results obtained from the elemental analysis.

3.3. Catalytic Studies. The catalytic activity, selectivity, and stability of the Fe-SBA products are tested for the liquid phase benzylation of benzene by BC, which holds the key importance for the production of diphenylmethane (DPM) or related compounds in pharmaceutical or fine chemical industry.[44,45] Figure 11 shows the conversion of various samples after a short reaction time of 20 min under a mild reaction temperature of 348 K. It is seen that the catalytic activity is evidently increased with iron loading. For example, when the iron loading increases from 1.2 to 4.1 wt %, the conversion of benzyl chloride is dramatically improved from 22.9 to 92.5%. For the almost linear increase of catalytic activity as a function of the iron content at low loadings, one possible reason is that both isolated and low polymeric iron species are reactive iron species in alkylation reactions.[42,46−49] In comparison to Fe-SBA(4), sample Fe/SBA(4) obtained by conventional incipient wetness impregnation can only afford a much lower alkylation

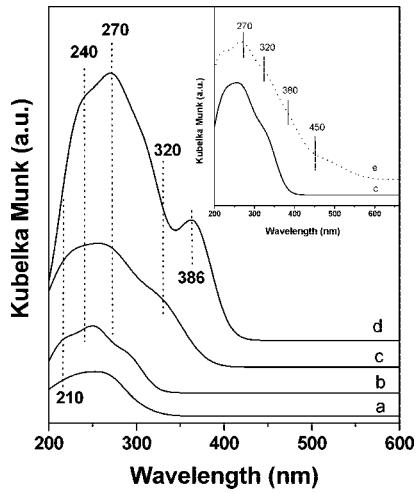

Figure 8. Diffuse reflectance UV−vis spectra of various Fe-loaded SBA-15 materials: (a) Fe-SBA(1); (b) Fe-SBA(2); (c) Fe-SBA(4); (d) Fe-SBA(8). Inset compares the spectra of the (c) Fe-SBA(4) and (e) Fe/SBA(4) catalysts.

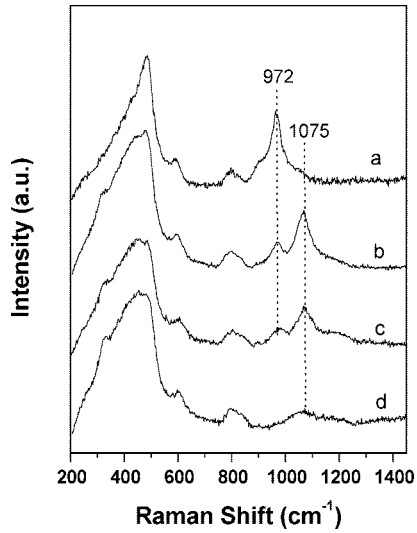

Figure 9. UV-Raman spectra of (a) cal-SBA-15, (b) Fe-SBA(1), (c) Fe-SBA(4), and (d) Fe/SBA(4) catalysts excited by the 325-nm laser line.

efficiency in terms of BC conversion and selectivity toward DPM under the same reaction conditions. This observation, together with the marginal decrease in the BC conversion from the Fe-SBA(8) sample, indicates that small oligomeric Fe_xO_y clusters and "bulklike" iron oxide nanoparticles are much less reactive iron species than the isolated or low polymeric iron species in alkylation reactions.

Figure 12 shows the conversion of BC with reaction time on iron-containing SBA samples at 348 K. Surprisingly, the samples Fe-SBA(4) still show excellent catalytic activity although the catalyst loading is 5 times decreased. For example, Fe-SBA(4) shows 100% conversion of benzyl chloride after a reaction time of 30 min, and Fe-SBA(8) gives 100% conversion after a reaction time of 45 min. This behavior can be explained by a five-times lower number of active sites, which induces a reduced contact time between reactants/products and the solid and thus a faster desorption of the products out of the solid.[50] Moreover, the selectivity for DPM on the two samples is above 99% at a complete benzyl chloride conversion. These results indicate a large amount of catalytic active sites in Fe-SBA(4). Additionally, it has been clarified that the rate data for the benzylation of

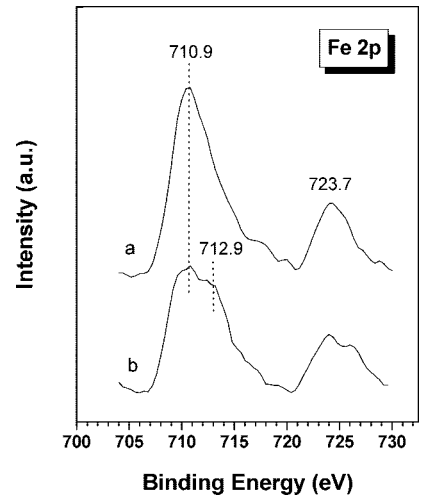

Figure 10. Fe 2p core-level spectra of (a) Fe-SBA(4) and (b) Fe/SBA(4) samples.

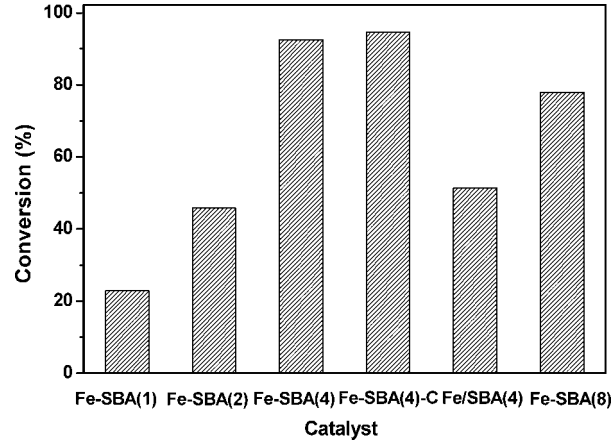

Figure 11. Conversion of benzyl chloride on various samples after a reaction time of 20 min at 348 K (catalyst load of 0.1 g).

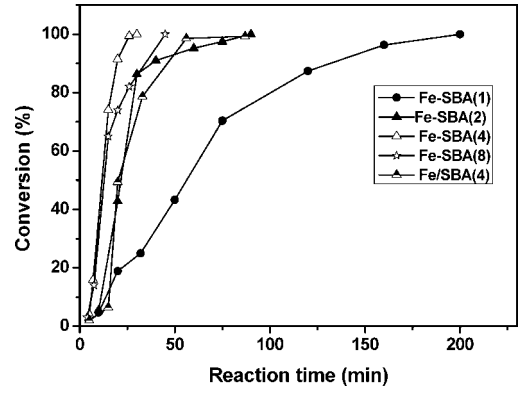

Figure 12. Conversion of BC with reaction time on various samples at 348 K (catalyst load of 0.02 g).

benzene reaction in excess benzene over the Fe-SBA catalysts can be well fitted by the pseudofirst-order rate kinetics.[18] As could be seen from Table 2, the apparent rate constants for the different catalysts decline in the following order: Fe-SBA(4) > Fe-SBA(8) > Fe-SBA(2) > Fe/SBA(4) > Fe-SBA(1). Similar trend for the benzylation of benzene has also been reported in Fe-modified mesoporous materials obtained by direct hydrothermal synthesis.[18] The apparent rate constant (k_a) for the benzylation reaction over Fe-SBA(4) is 1.569×10^{-4} min^{-1}

TABLE 2: Properties of the Catalysts in the Benzylation of Benzene Using Benzyl Chloride at 348 K[a]

catalyst[b]	time[c] (min)	selectivity[d] (%)	rate constant $K_a \times 10^{-4}$ (min^{-1})
Fe-SBA(1)	200	100	188
Fe-SBA(2)	90	100	816
Fe-SBA(4)	30	98.9	1569
Fe-SBA(8)	45	90.3	848
Fe/SBA(4)	90	87.4	579

[a] Reaction conditions: benzene:benzyl chloride = 15:1 (molar ratio). [b] Amount of catalyst: 20 mg. [c] Time required for complete conversion of benzyl chloride. [d] Selectivity to DPM.

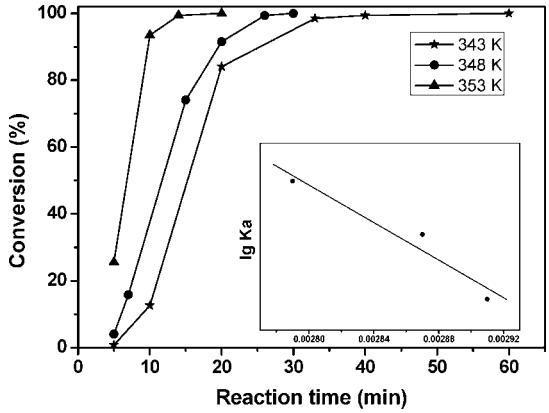

Figure 13. Effect of reaction temperature on the conversion of benzyl chloride in the benzylation of benzene over Fe-SBA(4) catalyst (catalyst load of 0.02 g).

TABLE 3: Effect of Reaction Temperature over Fe-SBA(4) Catalyst in the Benzylation of Benzene with BC[a]

reaction temperature (K)[b]	time[c] (min)	selectivity[d] (%)	rate constant $K_a \times 10^{-4}$ (min^{-1})
343	60	100	560
348	30	98.9	1569
353	20	96.4	2079

[a] Reaction conditions: benzene:benzyl chloride = 15:1 (molar ratio). [b] Amount of catalyst: 20 mg. [c] Time required for complete conversion of BC. [d] Selectivity to DPM.

and that of Fe-SBA(8) is 848 $\times$ 10^{-4} min^{-1}, while Fe/SBA-15(4) registers an apparent rate constant of only 579 $\times$ 10^{-4} min^{-1}.

To further evaluate the catalytic performance of Fe-SBA(4), its catalytic reactivity was tested at both lower and higher temperatures. Figure 13 shows the effect of the reaction temperature on catalytic activity. The product selectivity is given in Table 3. Obviously, a decrease of reaction temperature led to a decrease of catalytic activity. For example, at 353 K the reaction is completed after a very short reaction time of 20 min, whereas a much longer reaction time of 60 min is needed for complete BC conversion at 343 K. Similarly, the apparent rate constant k_a decreased from 2.079 $\times$ 10^{-4} min^{-1} at 353 K to 560 $\times$ 10^{-4} min^{-1} at 343 K. Only a slight change in the selectivity for DPM is observed, and a selectivity always high above 98.4% for DPM can be achieved at all the reaction temperatures used in this study. The higher dialkylation selectivity as found in our study is understandable when considering the fact that the present results were obtained under reaction conditions with much higher benzene to BC ratios.[46,47] The first-order rate constants calculated from these curves give an Arrhenius plot (inset to Figure 12), indicating a value of the activation energy of 86.4 kJ mol^{-1} for the Fe-SBA(4) catalyst.

TABLE 4: Effect of Recycling of the Fe-SBA(4) Catalyst in the Benzylation of Benzene with BC at 348 K[a]

catalyst[b]	time[c] (min)	selectivity (%)[d]	rate constant $K_a \times 10^{-4}$ (min^{-1})
fresh	30	98.9	1569
first reuse	30	98.5	1564
second reuse	30	98.4	1572
second reuse[e]	60	96.5	837
sixth reuse	29	97.6	1562

[a] Reaction conditions: benzene:benzyl chloride = 15:1 (molar ratio). [b] Amount of catalyst: 20 mg. [c] Time required for complete conversion of BC. [d] Selectivity to DPM. [e] Used catalyst without regeneration by calcination at 823 K.

Finally, the reusability of Fe-SBA(4) was also evaluated. The results are presented in Table 4. It is found that there is no difference in either activity or selectivity between the first and sixth runs (Table 4, entries 2 and 5). Fe leaching is negligible during the above recycles. It is also interesting to note that the well-ordered hexagonal arrays of mesopores (1D channels) of the Fe-SBA(4) could be well maintained in the used Fe-SBA(4) catalyst (see Figure S2). This allows confirmation that the hexagonal pore structure of Fe-SBA(4) material was robust enough to survive the selective alkylation process. Such catalytic characteristic is of great importance for potential industrial application. It is important to remark that the Fe-SBA(4) catalyst has to be regenerated by recalcination of the used catalyst in flowing air at 823 K for 2 h to maintain the activity through the consecutive runs. Apparently recalcinations are effective because they get rid of the organic species strongly adsorbed on the catalyst surface that ultimately lead to catalyst deactivation. In fact, if reuse is attempted without recalcination, the catalytic activity of Fe-SBA(4) is dramatically reduced (Table 4, entry 4).

3.4. Discussion. Our results demonstrate that the new process, involving the propagation of the $OH^{\bullet}$ radicals, oxidizing and removing the template via Fenton-based processing, followed by simultaneous Fe incorporation into the SBA-15 is highly effective for the direct synthesis of iron-containing large-pore hexagonal SBA-15 materials. Iron-containing mesoporous materials have attracted considerable recent attention owing to their unique molecular adsorption, redox, and catalytic properties in many industrially important reactions.[3,4,51] However, the incorporation of Fe into the framework of SBA-15 synthesized is particularly challenging, apparently due to the difficulty of the formation of Fe−O−Si bonds under strongly acidic synthesis conditions.[22,41] The most apparent advantage of the present integrated detemplation−incorporation method based on Fenton-chemistry ($Fe^{2+}-H_2O_2$) is that it avoids high-temperature calcination of the material thus minimizing the structural shrinkage as well as the reduction in time and steps in the preparation route. Additionally, this method can allow the controlled dispersion of a higher amount of iron oxide species on the surface of the mesoporous host, thus providing a new, attractive alternative for preparing defined transition metal modified mesoporous catalyst systems with more favorable textural properties.

TGA and DRIFTS results reveal that, the complete template removal can be easily achieved by Fenton treatment of the organic-containing SBA-15 hosts at low temperature in a short time of 2 h. On considering that the Fenton process ($Fe^{2+} + H_2O_2 \rightarrow Fe^{3+} + {}^{-}OH + {}^{\bullet}OH$) is a powerful advanced oxidation technology to remove organic pollutants from wastewater,[26] it is reasonable that the effective and complete detemplation can

be achieved under such mild conditions. It is assumed that the •OH radicals generated by Fenton reaction involving hydrogen peroxide and Fe^{2+} in solution are able to oxidize the template at low temperature. This result is in agreement with the recent work by Melián-Cabrera et al.,[29] who reported that detemplation of zeolite beta (BEA) can be successfully achieved at room temperature by catalytic oxidation of the occluded templates using H_2O_2 in the presence of trace amounts of Fe^{3+}. A recent work by Xia and Mokaya[52] has also described the use of H_2O_2-mediated Fenton-type oxidation as a promising method for generating surfactant-free mesoporous materials with molecular ordering and high textural properties under mild conditions. In contrast to the way in which only a simple detemplation step is realized in previous studies,[29,52] it should be stressed that the Fenton's reagent ($Fe^{2+}-H_2O_2$) employed in the present case is more attractive for a facile simultaneous detemplation and Fe-incorporation into as-synthesized surfactant-containing mesoporous silica materials.

On the other hand, investigation by means of UV−vis DRS has confirmed that, at low Fe content (below 1.9 wt %), the surface of Fe-SBA is mainly covered by highly dispersed tetrahedral framework Fe^{3+} species and isolated extraframework iron species. At higher Fe loading, isolated extraframework iron species become more abundant, and at 8.9 wt %, small oligomeric Fe_xO_y clusters due to a further polymerization of the Fe species also appears. The fact that no significant absorption above 400 nm is observed for all Fe-SBA samples indicates that the as-synthesized materials are free from bulk ferric oxide. On the other hand, UV resonance Raman experiments showed bands in the region of 1000−1200 cm^{-1} associated with the presence of isolated Fe species incorporated in the framework. Very recently, on investigating the effect of aluminum on the nature of the iron species in Fe−Al−SBA-15, Li and co-workers attributed the resonance Raman bands at 1090 and 1140 cm^{-1} to the isolated tetrahedral Fe ions in the silica framework and extraframework, respectively.[41] It follows that the absence of such resonance bands in the Fe/SBA(4) sample may be rationalized by the significant enhanced absorption in the ultraviolet region due to the presence of substantial fraction of "bulklike" Fe_2O_3 species in this material. All these facts, coupled with the XPS data, suggest that the impregnation method is not suitable to prepared catalysts with highly isolated catalytic active sites and the metal oxides tend to appear in the channel or external surface of the products as byproducts which would jam the channel or play a negative role in catalysis.[43]

At this juncture, it is also important to note that, owing to the intrinsic mild nature of the above Fenton-based template removal procedure, strong silica cross linkage may not be achieved in the final material thus lacking sufficient structural stability for practical applications. It is therefore of high interest to make a further investigation of the present Fe-SBA material subjected to a further calcination at elevated temperatures. As is clear from Figure 11, subsequent thermal treatment of the as-synthesized sample Fe-SBA(4) at 823 K was beneficial for the catalytic efficiency, which was ascribed to the enhanced hydrophobicity and well maintained textural properties (Table 1) of the calcined material. The hydrophobicity of the calcined material favored the adsorption and discharge of the reactants or products. This demonstrates that, from a practical point of view, postcalcination treatment can be used as an effective means to further improve the catalytic efficiency of the present Fenton-detemplated material.

Although the main purpose of this work was to present a novel method for preparing higher loaded Fe-SBA-15 catalysts with high iron dispersion and improved textural properties, we would like to focus here on the mechanisms that may be considered to explain the overall detemplation−incorporation process. In the conventional Fenton process the central event is the reaction between ferrous ions and hydrogen peroxide, producing hydroxyl radicals with powerful oxidizing abilities.[26−28] Despite its proven effectiveness, in most cases, a final separation of soluble iron species in the form of iron sludge from the treated water is needed to avoid second contamination.[26,28] Under our detemplation−incorporation conditions, the complete degradation of organic surfactants into carbon dioxide and water can be achieved in several hours. Simultaneously, the soluble iron species could be adsorbed over the catalyst surface, probably at the liberated silanol sites. This may lead to the generation of a new type of heterogeneous Fenton-type catalyst, which is supposed to be more active than the conventional homogeneous Fenton reagent,[53] thus accelerating the overall efficiency for template removal. All these factors result in the facile removal of the organic templates and incorporation of Fe ions during Fenton processing at the molecular level. In this sense, these findings formed the basis for the creation of the new method for the facile synthesis of iron oxides or other transition metal oxides in confined environments.

4. Conclusions

We have successfully developed a combined detemplation−incorporation method for the facile and direct synthesis of iron-containing large-pore hexagonal SBA-15 materials at low temperature. The as-synthesized Fe-SBA materials show excellent performance on benzylation of benzene using BC as the alkylating agent. By use of this method, different amounts of iron into the mesoporous structure can be incorporated by simply varying the concentration of the initial ferrous solution. The amount of Fe incorporated is higher than with most procedures without damaging the properties of the parent material and avoiding the formation of bulk iron oxide outside the porous structure. The SBA-15 structure is retained by the presence of iron species, possibly due to an efficient template removal by avoiding high temperature calcination of the material. The TEM and EDS results together with XRD experiments confirm that iron is present within the silica pores. N_2 sorption results indicate that both high surface area and large pore volume are well maintained for Fe-SBA-15. UV Raman shows some Fe is incorporated in the framework and UV−vis diffuse reflectance spectroscopy analysis confirms the presence of both framework and extraframework Fe with tetrahedral coordination. The most apparent advantage of the present detemplation−incorporation methodology are the reduction in time and steps in the preparation route as well as an improved dispersion and catalytic activity of the metal oxide species, which may offer new routes for the in situ synthesis of iron oxides or other transition metal oxides in confined environments.

Acknowledgment. This work was supported by the NSF of China (20421303, 20473021, and 20633030), the State Key Basic Research Program of PRC (2003CB615807), the National High Technology Research and Development Program of China (2006AA03Z336), the Shanghai Science & Technology Committee (07QH14003), and Shanghai Education Committee (06SG03).

Supporting Information Available: Figures depicting the high-angle X-ray diffraction patterns of various Fe-loaded SBA-

15 materials and THE TEM image of sample Fe-SBA(4) after four rounds of recycling tests. This material is available free of charge via the Internet at http://pubs.acs.org.

References and Notes

(1) Corma, A. *Chem. Rev.* **1997**, *97*, 2373.
(2) Davis, M. E. *Nature* **2002**, *417*, 813.
(3) Kresge, C. T.; Leonowicz, M. E.; Roth, W. J.; Vartuli, J. C.; Beck, J. S. *Nature* **1992**, *359*, 710.
(4) Beck, J. S.; Vartuli, J. C.; Roth, W. J.; Leonowicz, M. E.; Kresge, C. T.; Schmitt, K. D.; Chu, C. T. W.; Olson, D. H.; Sheppard, E. W. *J. Am. Chem. Soc.* **1992**, *114*, 10834.
(5) Kim, J. Y.; Yoon, S. B.; Yu, J. S. *Chem. Mater.* **2003**, *15*, 1932.
(6) Huo, Q.; Leon, R.; Petroff, P. M.; Stucky, G. D. *Science* **1995**, *268*, 1342.
(7) Vaudry, F.; Khodabandeh, S.; Davis, M. E. *Chem. Mater.* **1996**, *8*, 1451.
(8) Zhao, D. Y.; Feng, J. L.; Huo, Q. S.; Melosh, N.; Fredrickson, G. H.; Chmelka, B. F.; Stucky, G. D. *Science* **1998**, *279*, 548.
(9) Dufaud, V.; Davis, M. E. *J. Am. Chem. Soc.* **2003**, *125*, 9403.
(10) Jarupatrakorn, J.; Tilley, T. D. *J. Am. Chem. Soc.* **2002**, *124*, 8380.
(11) Liu, Y. M.; Cao, Y.; Zhu, K. K.; Yan, S. R.; Dai, W. L.; He, H. Y.; Fan, K. N. *Chem. Commun.* **2002**, 2832.
(12) Liu, Y. M.; Cao, Y.; Yi, N.; Feng, W. L.; Yan, S. R.; Dai, W. L.; He, H. Y.; Fan, K. N. *J. Catal.* **2004**, *214*, 417.
(13) Taguchi, A.; Schüth, F. *Microporous Mesoporous Mater.* **2005**, *77*, 1.
(14) Groothaert, M. H.; van Bokhoven, J. A.; Battiston, A. A.; Weckhuysen, B. M.; Schoonheydt, R.A. J. *Am. Chem. Soc.* **2003**, *125*, 7629.
(15) Groothaert, M. H.; Smeets, P. J.; Sels, B. F.; Jacobs, P. A.; Schoonheydt, R. A. *J. Am. Chem. Soc.* **2005**, *127*, 1394.
(16) Jarry, B.; Launay, F.; Nogier, J. P.; Montouillout, V.; Gengembre, L.; Bonardet, J. L. *Appl. Catal., A* **2006**, *309*, 177.
(17) Yue, Y.; Gideon, A.; Bonardet, J. L.; Melosh, N.; D¢Espinose, J. B.; Fraissard, J. *Chem. Commun.* **1999**, 1967.
(18) Vinu, A.; Sawant, D. P.; Ariga, K.; Hossain, K. Z.; Halligudi, S. B.; Hartmann, M.; Nomura, M. *Chem. Mater.* **2005**, *17*, 5339.
(19) Nozaki, C.; Lugmair, C. G.; Bell, A. T.; Tilley, T. D. *J. Am. Chem. Soc.* **2002**, *124*, 13194.
(20) Zhang, W. H.; Lu, J.; Han, B.; Li, M.; Xiu, J.; Ying, P.; Li, C. *Chem. Mater.* **2002**, *14*, 3413.
(21) Berrichi, Z. E.; Cherif, L.; Orsen, O.; Fraissard, J.; Tessonnier, J. P.; Vanhaecke, E.; Louis, B.; Ledoux, M.-J.; Pham-Huu, C. *Appl. Catal., A* **2006**, *298*, 194.
(22) Li, Y.; Feng, Z. C.; Lian, Y. X.; Sun, K. Q.; Zhang, L.; Jia, G. Q.; Yang, Q. H.; Li, C. *Microporous Mesoporous Mater.* **2005**, *84*, 41.
(23) Byambajav, E.; Ohtsuka, Y. *Appl. Catal., A* **2003**, *252*, 193.
(24) Wang, X.; Zhang, Q.; Guo, Q.; Lou, Y.; Yang, L.; Wang, Y. *Chem. Commun.* **2004**, 1396.
(25) Murugavel, R.; Roesky, H. W. *Angew. Chem., Int. Ed.* **1997**, *109*, 491.
(26) Meri, S.; Selcuk, H.; Gallo, M.; Belgiorno, V. *Desalination* **2005**, *173*, 239.
(27) Han, Y. F.; Phonthammachai, N.; Ramesh, K.; Zhong, Z.; White, T. *Environ. Sci. Technol.* **2008**, *42*, 908.
(28) Laat, J. D.; Le, T. G. *Appl. Catal., B* **2006**, *66*, 137.
(29) Melián-Cabrera, I.; Kapteijn, F.; Moulijn, J. A. *Chem. Commun.* **2005**, 2178.
(30) Wang, Y. M.; Wu, Z. Y.; Shi, L. Y.; Zhu, J. H. *Adv. Mater.* **2005**, *17*, 323.
(31) Kleiz, F.; Schmidt, W.; Schüth, F. *Microporous Mesoporous Mater.* **2003**, *65*, 1.
(32) Tian, B. Z.; Liu, X. Y.; Yu, C. Z.; Gao, F.; Zhao, D. Y. *Chem. Commun.* **2002**, 1186.
(33) Liu, Y. M.; Feng, W. L.; Li, T. C.; He, H. Y.; Dai, W. L.; Cao, Y.; Fan, K. N. *J. Catal.* **2006**, *239*, 125.
(34) Geidel, E.; Lechert, H.; Döbler, J.; Jobic, H.; Calzaferri, G.; Bauer, F. *Microporous Mesoporous Mater.* **2003**, *65*, 31.
(35) Zhou, R.; Cao, Y.; Yan, S. R.; Deng, J. F.; Liao, Y. Y.; Hong, B. F. *Catal. Lett.* **2001**, *107*, 75.
(36) Berndt, H.; Martin, A.; Brückner, A.; Schreier, E.; Müller, D.; Kosslick, H.; Wolf, G.-U.; Lücke, B. *J. Catal.* **2000**, *191*, 384.
(37) Solsona, B.; Blasco, T.; Nieto, J. M. L.; Peña, M. L.; Rey, F.; Vidal-Moya, A. *J. Catal.* **2001**, *203*, 443.
(38) Wang, X. Q.; Ge, H. L.; Jin, H. X.; Cui, Y. J. *Microporous Mesoporous Mater.* **2005**, *86*, 335.
(39) Bordiga, S.; Buzzoni, R.; Geobaldo, F.; Lamberti, C.; Giamello, E.; Zecchina, A.; Leofanti, G.; Petrini, G.; Tozzola, G.; Vlaic, G. *J. Catal.* **1996**, *158*, 486.
(40) Tuel, A.; Acrorn, I.; Millet, J. *J. Chem. Soc. Faraday Trans.* **1998**, *94*, 43501.
(41) Li, Y.; Feng, Z. C.; Xin, H. C.; Fan, F. T.; Zhang, J.; Li, C. *J. Phys. Chem. B* **2006**, *110*, 26114.
(42) Wang, X. X.; Wang, Y.; Tang, Q. H.; Guo, Q.; Zhang, Q. H.; Wan, H. L. *J. Catal.* **2003**, *217*, 457.
(43) Vinu, A.; Krithiga, T.; Balasubramanian, V. V.; Asthana, A.; Srinivasu, P.; Mori, T.; Ariga, K.; Ramanath, G.; Ganesan, P. G. *J. Phys. Chem. B* **2006**, *110*, 11924.
(44) Olah, G. A. *Friedel-Crafts Chemistry*; Wiley: New York, 1973.
(45) Khadilkar, B. M.; Borkar, S. D. *Chem. Technol. Biotechnol.* **1998**, *71*, 209.
(46) Cseri, T.; Békássy, S.; Figueras, F.; Rizner, S. *J. Mol. Catal., A: Chem.* **1995**, *98*, 101.
(47) Pai, S. G.; Bajpai, A. R.; Deshpande, A. B.; Samant, S. D. *J. Mol. Catal. A: Chem.* **2000**, *156*, 233.
(48) Bachari, K.; Millet, J. M. M.; Benaïchouba, B.; Cherifi, O.; Figueras, F. *J. Catal.* **2004**, *221*, 55.
(49) Bachari, K.; Millet, J. M. M.; Bonville, P.; Cherifi, O.; Figueras, F. *J. Catal.* **2007**, *249*, 52.
(50) Sun, Y.; Walspurger, S. P.; Tessonnier, J.-P.; Louis, B.; Sommer, J. *Appl. Catal., A* **2006**, *300*, 1.
(51) Selvaraj, M.; Pandurangan, A.; Seshadri, K. S.; Sinha, P. K.; Krishnasamy, V.; Lal, K. B. *J. Mol. Catal. A: Chem.* **2002**, *186*, 173.
(52) Xia, Y. D.; Mokaya, R. *J. Phys. Chem. B* **2006**, *110*, 9122.
(53) Melero, J. A.; Calleja, G.; Martínez, F.; Molina, R.; Pariente, M. I. *Chem. Eng. J.* **2007**, *131*, 245.

JP802202V